Multiband Single-Layer Frequency Selective Surface Designed by Combination of Genetic Algorithm and Geometry-Refinement Technique

Masataka Ohira, *Student Member, IEEE*, Hiroyuki Deguchi, *Member, IEEE*, Mikio Tsuji, *Member, IEEE*, and Hiroshi Shigesawa, *Fellow, IEEE*

***Abstract*—This paper proposes an optimization-design method for the frequency selective surface (FSS) based on the genetic algorithm (GA) incorporated with a geometry-refinement technique. The present method takes the connectivity condition of the elements into consideration, thereby resulting in an easy fabrication. As an example, we design the multiband single-layer FSS for transmitting *L* band (1.5 GHz band) and *S* band (2.5 GHz band) and also reflecting *Ka* band (20/30 GHz band). The designed FSS has bandwidths broader than previous FSSs. Finally, the validity of the present method is proved by the agreement between the calculated and the measured transmission responses for the designed FSS.**

***Index Terms*—Broadband, frequency selective surface (FSS), genetic algorithm (GA), geometry-refinement technique, multiband.**

I. Introduction

FREQUENCY selective surfaces (FSSs) are widely used as subreflectors for the satellite communication so that a single main reflector can share the different frequency bands. To increase the capabilities of multifunction and multifrequency antennas, a subreflector equipped with FSS is required to operate at multifrequency bands.

The multilayering of FSSs was first employed to realize the multiband operation. Recently, the global optimizer genetic algorithm (GA) [1], [2] has been applied to the design of complex multilayered FSSs [3], [4]. Also the single-layer FSSs having the dual-resonant elements have been investigated. They are light in weight and compact in volume, compared with the multilayered FSSs. The elements proposed so far are an array of two different-length dipoles [5], concentric rings [6], [7], double square loops [8], [9], fractal shapes [10], [11], and so on. However, the FSS with two different-length dipoles is dependent on the polarization of the incident wave and also the double-loop types are restricted on the bandwidth. Fractal FSSs realize only the octave separation between two reflection bands. Thus, the single-layer FSSs with these simple-element shapes can not have the same characteristics as the multilayered ones. Therefore an optimization-design technique, based on the GA in conjunction with the method of moments (MoM) [12], [13], has been applied to the design of the arbitrary element shape for not only the multilayered FSSs but also for the single-layer FSSs [14], [15].

However, the element shapes obtained by the GA are more complicated than those of previous FSSs. Especially, if no geometrical constraints are given to the GA-designed element shapes, most of the FSS element shapes include critical points, which mean that the adjacent conductors touch each other only at the lattice point generated by discretizing the unit cell into the grid for the analysis. As a result, the fabricated FSS has the frequency characteristics different from the designed FSS at the specified bands because the resonant electrical length of the element is changed, depending on the contact condition between conductors at critical points. As a result, FSS element shapes should avoid having any point-contact conductors.

This paper proposes an FSS design method based on the GA with a geometry-refinement method (GRM), which is a new-type of operator for refining element shapes. In Section II, we develop the geometry-refinement technique, which operates on two-dimensional (2-D) arrays. This operator can remove the critical points in the elements not by natural selection and evolution, but by forcing to eliminate them. In Section III, it is shown that by the present method, optimum FSS elements can be obtained faster than the conventional GA (CGA) technique using natural selection and evolution. In Section IV, we show a design example of multiband single-layer FSS for transmitting *L* band (1.5 GHz band) and *S* band (2.5 GHz band) and also reflecting *Ka* band (20/30 GHz band). The designed FSS has bandwidths broader than previous FSSs. Finally the effectiveness of the present design method is confirmed experimentally.

II. Design Method

A. Optimization of Element Shape

Fig. 1 shows a single-layer FSS without a dielectric substrate under consideration and the unit cell of its periodic structure extended infinitely. The unit cell is divided into $N \times M$ discretization (16×16 discretization is handled in this paper as well as [14]) to represent the FSS with an arbitrary element shape in terms of 1s and 0s in the GA. The 1 and 0 correspond to the perfect conductor plate (hatched pixels in Fig. 1) and the free space (blank pixels), respectively. In the present method, the unit-cell geometry has four-fold symmetry to work for dual polarizations. So, the GA operates on one quarter of the unit-cell geometry, and the region is encoded into a 64 bit binary string. The GA starts with a random population and then generates the

Manuscript received May 7, 2003; revised February 18, 2004. The work was supported in part by a Grant-in Aid for Scientific Research C 2 13650439 from the Japan Society for the Promotion of Science and by the Aid of Doshisha University's Research Promotion Fund.

The authors are with the Department of Electronics, Doshisha University, Kyoto 610-0321, Japan (e-mail: etd1103@mail4.doshisha.ac.jp).

Digital Object Identifier 10.1109/TAP.2004.835289

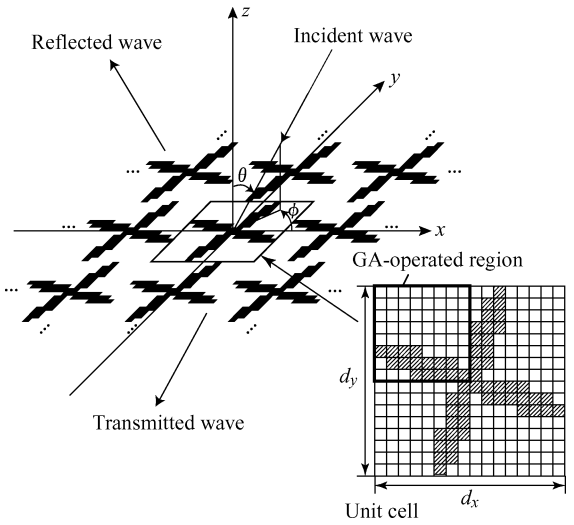

Fig. 1. Single-layer FSS and GA-operated region.

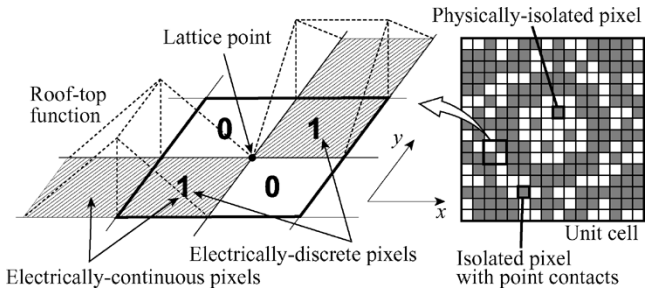

Fig. 2. Relation between basis functions for the analysis and 0s and 1s for GA-optimization at a lattice point.

FSS element shapes through selection, crossover, mutation and one more operator proposed in this paper. Also the GA keeps the best individual after each generation (elitist strategy). The size of the unit cell ($d_x \times d_y$) must be determined not to yield the grating lobe in the specified bands.

B. Geometry-Refinement Technique

Not only typical GA operators but also a new-type of operator is needed for the optimization design of the FSS element shape taking into account the connectivity condition of the elements. We call hereafter this operator a GRM. The reason for introducing this new operator is mentioned below.

The relation of the basis functions for the analysis with 1s and 0s in the GA is shown in Fig. 2. Most of the FSS element shapes generated by the GA include the point contact of the conductors ($\begin{smallmatrix}0&1\\1&0\end{smallmatrix}$ and $\begin{smallmatrix}1&0\\0&1\end{smallmatrix}$) at the lattice points inside the unit cell and/or between adjacent cells, as shown in a unit-cell example of Fig. 2. If the conductors of an optimized FSS element have such points, it means that they do not touch each other analytically, but touch physically. As a result, the fabricated FSS may have the frequency characteristics different from the designed FSS at the specified bands, depending on the contact condition at the lattice point. The contact condition in the fabricated FSS may change drastically the resonant electrical length through the contact point. Therefore the lattice points of $\begin{smallmatrix}0&1\\1&0\end{smallmatrix}$ and $\begin{smallmatrix}1&0\\0&1\end{smallmatrix}$ become critical points when fabricating these elements. As a result, the FSS element should avoid having the point contact at the lattice point.

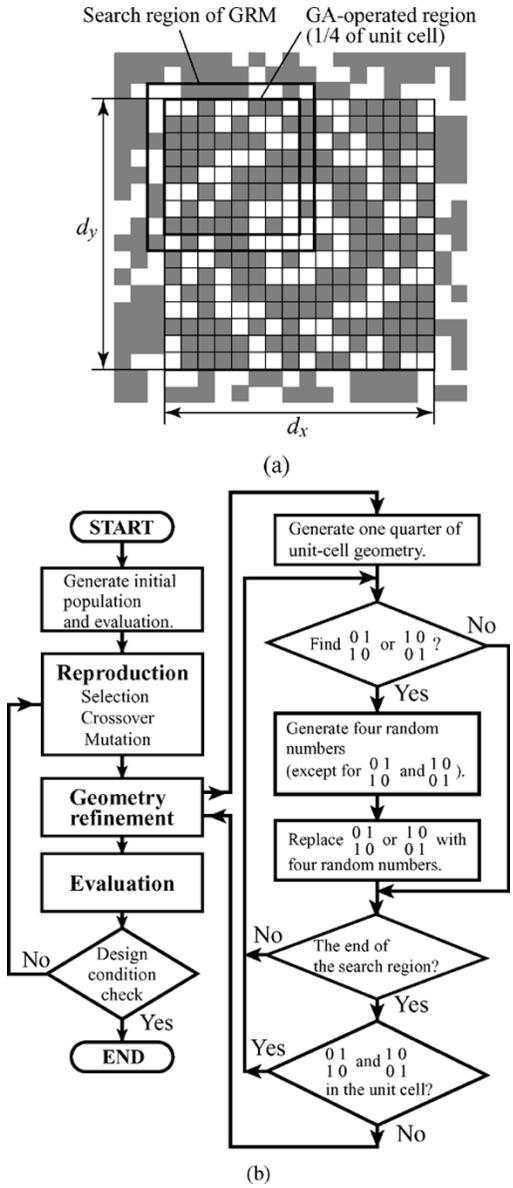

Fig. 3. Optimization-design method based on GA with GRM: (a) Search region of GRM and (b) flowchart of the present method.

TABLE I
SPECIFIED FREQUENCY BANDWIDTH

Transmission bands	L band (1.5 GHz)	1.525–1.559 GHz
	S band (2.5 GHz)	2.505–2.535 GHz
Reflection bands	Ka band (20 GHz)	17.7–21.2 GHz
	Ka band (30 GHz)	27.5–31.0 GHz

We propose here a GRM, which is a new operator for refining element shapes. Fig. 3 shows the flowchart of the optimization-design method based on the GA incorporated with the GRM. This operator removes the critical points not by natural selection and evolution of the GA, but by forcing to eliminate them. To keep four-fold symmetry of the element

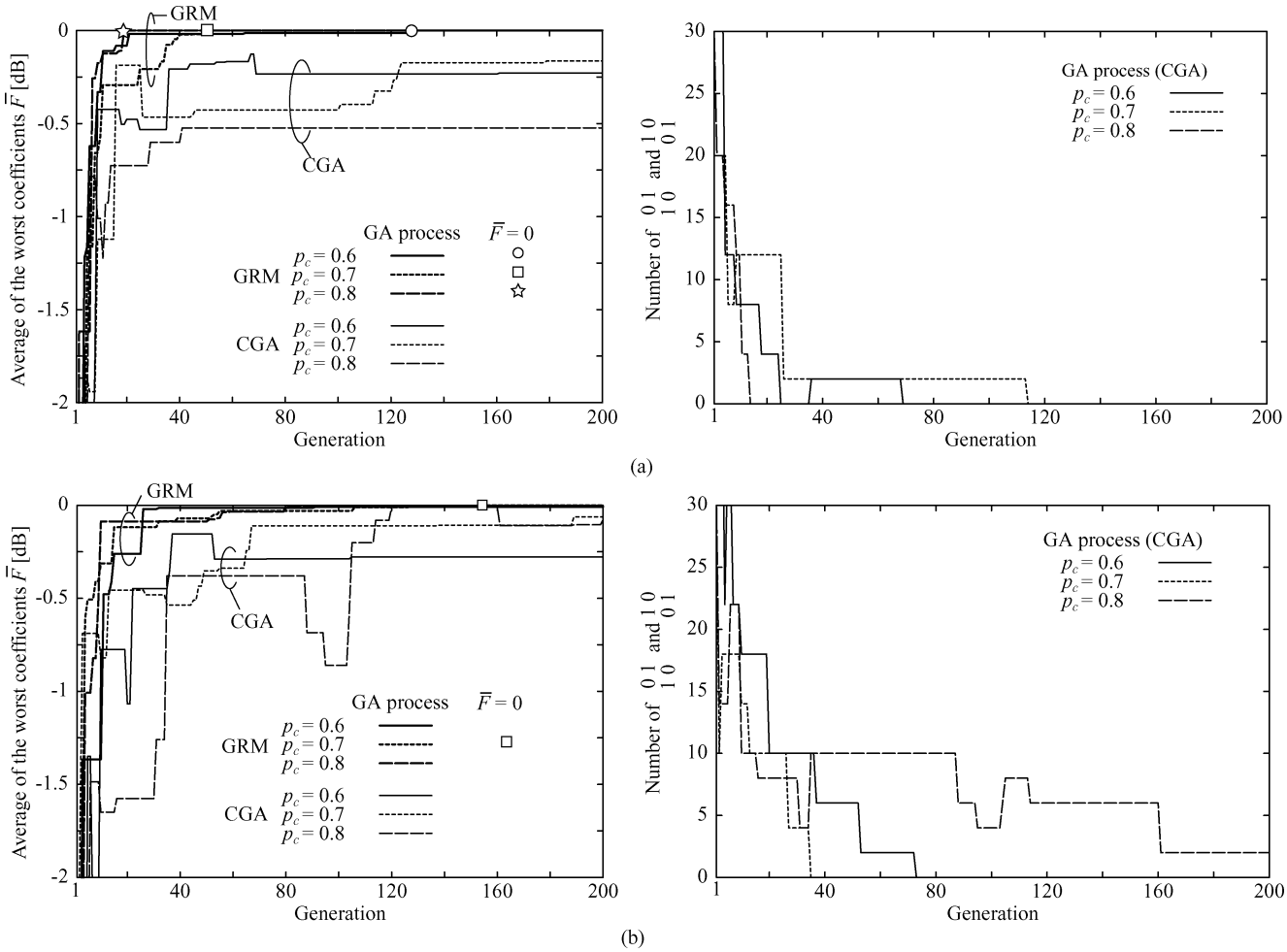

Fig. 4. Comparison of GA-optimization processes of the best individuals between the GRM and the CGA. (Figures on the left-hand side: average of the worst coefficients $\bar{F}$. Figures on the right-hand side: the number of the critical points): (a) Single-point crossover and (b) uniform crossover.

shapes, the GRM operates on one quarter of the unit cell and the boundaries (the search region in Fig. 3). After applying typical GA operators (selection, crossover and mutation), the GRM first finds 2-D arrays $\begin{matrix}0&1\\1&0\end{matrix}$ and $\begin{matrix}1&0\\0&1\end{matrix}$ (critical points) one after another from the left top of the search region, and then replaces these arrays with other 2-D arrays generated by random numbers. This routine is repeated until all the critical points are completely removed from the search region. The GRM is also applied to all the individuals which consist of random numbers at the first generation. It should be noted here that the GRM can also remove isolated pixels which have only the point contacts as shown in Fig. 2, but cannot remove physically-isolated pixels. However, even if the physically-isolated pixels exist in an optimized structure, we can ignore them physically and electrically because their currents can not be inherently modeled in the simulation. Thus, the GA selects the geometry-refined element with the desired specifications automatically.

C. Fitness Function

The characteristics of the FSSs generated by both typical GA operators and the GRM are evaluated according to the fitness value, which represents a measure of goodness. The fitness function is defined as

$$\text{fitness} = \frac{1}{1+\bar{F}} \tag{1}$$

where

$$\bar{F} = \frac{1}{N_f}\sum_{i=1}^{N_f} G_i \,[\text{dB}] \tag{2}$$

$$G_i = \begin{cases} \max\{|S(pol.,\theta) - S_i|\}, & |S| > |S_i| \\ 0, & |S| \le |S_i| \end{cases} \tag{3}$$

and N_f is the number of specified bands; S is the reflection or transmission coefficient in decibels within specified bands; $pol.$ is the polarization of incident wave (TE and TM waves); θ is the incident angle; S_i is the design goal of reflection or transmission coefficient in dB within the ith specified band.

To calculate the frequency responses of the FSS, the analysis of the FSS follows the well-established procedure based on the MoM that solves the electric field integral equation (EFIE) for the unknown current distribution on the arbitrary unit-cell geometry [12], [13]. The scattered field from the FSS due to the incident wave (wavenumber k_0) can be calculated from the induced currents on the conductor plates. So, we can express the

scattered electric field derived by enforcing Floquet's periodicity condition as follows:

$$\begin{bmatrix} E_x^{(s)}(x,y) \\ E_y^{(s)}(x,y) \end{bmatrix} = \sum_{p=-\infty}^{\infty} \sum_{q=-\infty}^{\infty} \begin{bmatrix} \tilde{G}_{xx} & \tilde{G}_{xy} \\ \tilde{G}_{yx} & \tilde{G}_{yy} \end{bmatrix} \cdot \begin{bmatrix} \tilde{J}_x(k_{xp}, k_{yq}) \\ \tilde{J}_y(k_{xp}, k_{yq}) \end{bmatrix} e^{jk_{xp}x} e^{jk_{yq}y} \quad (4)$$

where $E_x^{(s)}$ and $E_y^{(s)}$ represent the x and y components of the scattered electric field, respectively. The transformed derivatives, the dyadic spectral Green's function and their constants are incorporated into $\tilde{G}_{xx}$, $\tilde{G}_{xy}$, $\tilde{G}_{yx}$ and $\tilde{G}_{yy}$ to simplify the notation. The details are omitted (see [12] and [13]). The wavenumber k_{xp} and k_{yq} can be expressed as $k_{xp} = k_0 \sin\theta\cos\phi + 2\pi p/d_x$ and $k_{yq} = k_0 \sin\theta \sin\phi + 2\pi q/d_y$, respectively. The indices (p, q) represents Floquet's harmonics. $\tilde{J}_x$ and $\tilde{J}_y$ are the Fourier transforms of x and y components J_x and J_y of the unknown currents. Applying the boundary condition $\boldsymbol{E}^{(i)} + \boldsymbol{E}^{(s)} = 0$ on the conductor plates to (4), we can solve unknown currents by using Galerkin's procedure for the unknown currents J_x and J_y expanded in terms of the roof-top basis functions as shown in Fig. 2. The reflection and transmission coefficients $S(pol., \theta)$ (in dB) are calculated from the known currents. Thus, G_i in (3) is the maximum difference between the desired characteristics S_i (in dB) and the worst reflection or transmission coefficient $S(pol., \theta)$ (in dB) in ith specified band. And, $\bar{F}$ in (2) simply means the average of the values of G_i in the desired frequency bands to reduce computational burden as well as [16]. If the fitness in (1) reaches 1.0 for the best individual in some generation, its unit-cell geometry is recognized as an optimum element shape. Otherwise the optimization cycle to next generation is repeated until an FSS with the desired characteristics is obtained.

III. Efficiency of Design Method

A. CGA Technique

The efficiency of the present method can be confirmed by comparing the convergence of $\bar{F}$ in (2) of the GRM for the generation with that of the CGA. For comparison, the CGA must search an optimum geometry without the critical points using natural selection and evolution. Therefore, the fitness function of the CGA evaluates the number of critical points in the unit cell in addition to the characteristics of FSS as follows:

$$\text{fitness} = \frac{1}{1 + \bar{F} + \beta P} \quad (5)$$

where the penalty P represents the number of critical points weighted by the coefficient β, and $\bar{F}$ is defined by (2).

As an example for checking the efficiency, we design the single-layer FSS for transmitting *L* band (1.5 GHz band) and *S* band (2.5 GHz band), and also reflecting *Ka* band (20/30 GHz band) as shown in Table I. Our design goals for the characteristics of the FSS are transmission coefficient -0.5 dB in the transmission bands and reflection coefficient -0.2 dB in the reflection bands for normal plane-wave incidence. The GA evaluates the transmission coefficient at 2.5 GHz in the transmission bands and the reflection coefficients at the frequency resolution of 0.5 GHz in the reflection bands. The unit-cell size is fixed to be $d_x = d_y = 8.0$ mm. The individuals are reproduced through the tournament selection, the crossover and the mutation. The GA performs the optimization by using the single-point or the uniform crossover with the rate p_c of 0.6–0.8. The mutation rate is chosen to be 0.05. The population size is fixed at 20 as the minimum size in which the GA works well for most of practical problems, and its size makes it possible to perform faster computation [1]. The weighting coefficient β decides the degree of the convergence between the characteristics $\bar{F}$ and the number of the critical points P. In this paper, to compare the results obtained by the CGA with those obtained by the GRM, a value of the weighting factor β is chosen so that both $\bar{F}$ and P can possibly approach the specified values within the generation number that the GRM needs to get the convergence. Therefore, the weighting coefficient β is chosen to be 0.1 because it is confirmed that both $\bar{F}$ and P for $\beta = 0.1$ converge much faster than those for both $\beta = 1.0$ and 0.01.

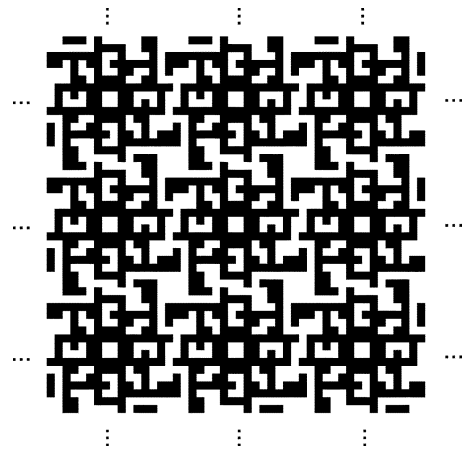

Fig. 5. Element shape of multiband single-layer FSS optimized by GA with geometry-refinement technique.

B. Comparison of Convergences

Fig. 4(a) and (b) shows the comparison of the GA-optimization processes of the best individuals between the GRM and the CGA using the single-point and the uniform crossovers. The figures on the left-hand side in Fig. 4 compare the values of $\bar{F}$ in (1) of the GRM with those in (5) of the CGA at each generation. And the figures on the right-hand side show the number of the critical points in both the unit cell and the boundaries in the CGA (the GRM that has no critical points is not shown). As shown in Fig. 4, the CGA greatly depends on both the method and the rate of the crossover, and yet can not obtain the FSSs that satisfy the given specifications by the 200th generation. On the other hand, the GA with the GRM obtains optimum geometries faster than the CGA. For $p_c = 0.6$ and 0.8 in Fig. 4(b), the GRM does not obtain the individual with $\bar{F} = 0$ by the 200th generation, but the values of $\bar{F}$ are very close to zero. Comparing the characteristics of FSSs at the 200th generation between the GRM and the CGA, the FSSs generated via the GRM have dual resonances at the specified reflection bands, while the solutions of the CGA do not always have dual resonances in all the GA-optimization

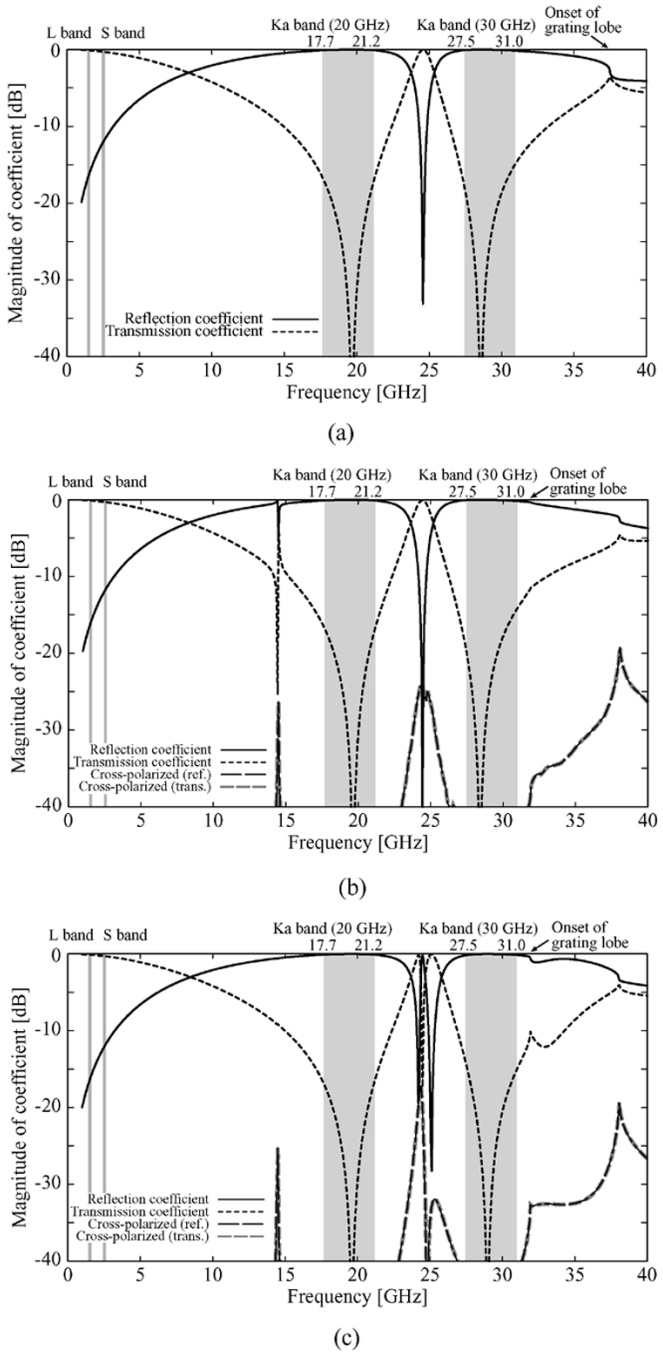

Fig. 6. Frequency characteristics of the multiband single-layer FSS illustrated in Fig. 5: (a) Normal incidence. (b) TE-wave incidence ($\theta = 10^\circ, \phi = 0^\circ$). (c) TM-wave incidence ($\theta = 10^\circ, \phi = 0^\circ$).

processes as long as the penalty P approaches zero within the generation number 200. That is, they are still local minima at the 200th generation, which do not completely fulfill the given specifications. It must take more generations for the CGA to explore an optimum solution. If the increase of the generation number is permitted and the penalty P is decreased gradually by adjusting the weighting coefficient β, the CGA may have the possibility to find an optimum geometry with a fitness almost equal to 1. So, it can be concluded that the GRM is not so sensitive for the GA parameters and more efficiently finds the optimum geometry, compared with the CGA.

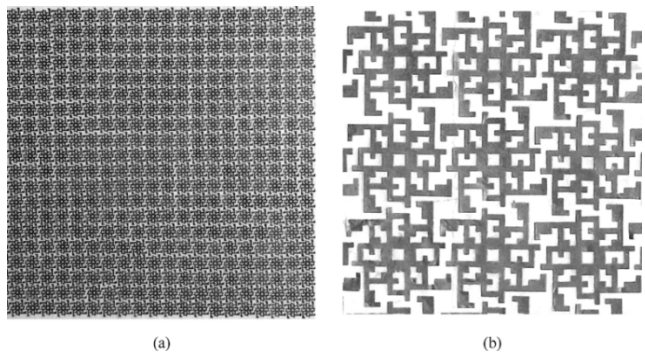

Fig. 7. Photographs of fabricated FSS: (a) Far view and (b) near view.

IV. Design and Experiments

A. Design of Multiband Single-Layer FSS

As a design example, we evaluate the frequency responses of the FSS not only for the normal plane-wave incidence and but also for both TE and TM wave incidences at the incident angle of $\theta = 10^\circ$. The specified bands and GA parameters are the same as those of the previous section. The single-point crossover with the rate of 0.8 is applied. Fig. 5 shows the element shape obtained through the GRM (3×3 cells in the infinite periodic structure). Its frequency characteristics are shown in Fig. 6. The designed FSS has the novel element shape, which satisfies the design goals for the frequency responses at the specified bands, independent of the angle and the polarization of the incident wave. Furthermore, the cross-polarized reflection and transmission coefficients are lower than -40 dB at the specified bands as shown in Fig. 6.

In Fig. 6, sharp dips appear out of the bands at 14.5 GHz for TE-wave oblique incidence and at 24.8 GHz for TM-wave oblique incidence. Not only the GA-designed FSS but also the dipole FSS has the similar sharp dips for the oblique incidence [17]. The sharp dips in the reflection characteristics are caused by anti-resonance. For the normal incidence, no radiation occurs at the anti-resonant frequency because the scattered waves are cancelled due to the complete-symmetric current distribution. The sharp transmission dips near the anti-resonance are caused by the modal interaction null [18], which can be easily understood from the equivalent circuit theory for connecting the anti-resonant reactive circuit with the resonant one.

Next, the bandwidths at two reflection bands are compared with those of previous multiband single-layer FSSs (for example, the convoluted double square loop FSS [9]). They have a fractional bandwidth of 0.15–0.25 at each band (the bandwidth refers to -10 dB level of the transmission coefficient), while the designed FSS has broader bandwidths of 0.37 at 20 GHz band and 0.23 at 30 GHz band. These bandwidths may not be obtained by previous dual-polarized and dual-resonant single-layer FSSs.

B. Experiments

Fig. 7(a) and (b) gives the far-view and the near-view photographs of the fabricated FSS for the measurement, respectively. Its element spacing is scaled up twice for the designed FSS. The fabricated FSS has 20×20 elements and its overall

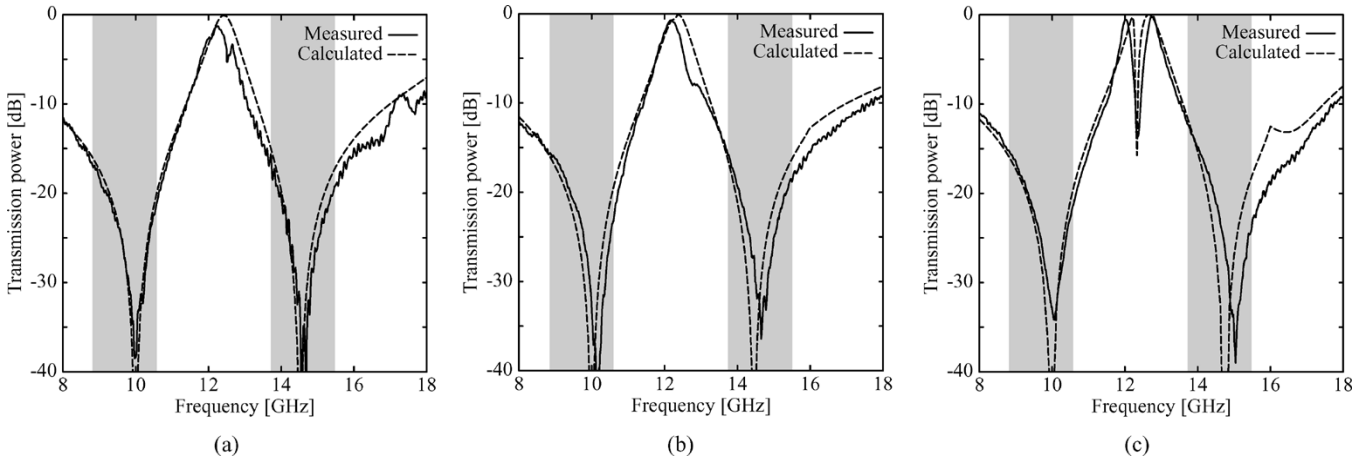

Fig. 8. Comparison of the transmission response between the measured and the calculated results: (a) Normal incidence, (b) TE-wave incidence ($\theta = 10^\circ$), and (c) TM-wave incidence ($\theta = 10^\circ$).

size is 320 mm $\times$ 320 mm. The measurements are performed at *X* and *Ku* bands. The sets of the standard gain horn antennas are used and the FSS is inserted between them. The distance between the antennas is determined so that the incident wave from the horn antenna can be assumed to be the plane wave on the FSS. The multiple-reflected wave between the FSS and the receive horn antenna causes a ripple on the measured results, of which the peak-to-peak level is about 2 dB at maximum. Therefore, transmission responses are measured by varying the distance between the FSS and the receive horn antenna at intervals of $\lambda/8$ (λ:wavelength). To suppress the ripple as much as possible on the measured results, the average values of the transmissions are employed.

Fig. 8 shows the comparison between the measured results (solid curves) and the calculated ones (dashed curves) for the normal incidence and the oblique incidences at the angle of $\theta = 10^\circ$. Both results agree very well, especially at the first resonant frequency in *X* band. It should be noted that the sharp null caused by the modal interaction null for TM-wave incidence is experimentally observed at the frequency of 12.2 GHz. At the higher band, the measured results slightly shift to higher frequency than the calculated ones because of the fabrication torelances of elements. Nevertheless, the agreement between the calculated and measured results proves the validity of the present method.

V. Conclusion

We have developed a multiband single-layer FSS using the optimization-design technique based on the GA into which the GRM is incorporated. This method takes the connectivity condition of the elements into account. The GRM can remove the critical points which mean that the adjacent conductors touch only at a point, so that the designed FSS without the point contacts of conductors can be easily fabricated. Furthermore, we have shown that the present method can obtain optimum FSS elements faster than the CGA technique using natural selection and evolution. As an example, we design the multiband single-layer FSS for transmitting *L* band (1.5 GHz band) and *S* band (2.5 GHz band) and also reflecting *Ka* band (20/30 GHz band). The designed FSS has a novel element shape, which shows the dual-resonant behavior. The characteristics of the obtained FSS are superior to those of previous FSSs in the bandwidth at two reflection bands. Finally, the validity of the present method has been proved by the agreement between the calculated and the measured transmission responses for the designed FSS.

Acknowledgment

The authors wish to thank the reviewers for their useful comments.

References

[1] J. M. Johnson and Y. Rahmat-Samii, "Genetic algorithms in engineering electromagnetics," *IEEE Antennas Propagat. Mag.*, vol. 39, pp. 7–25, Aug. 1997.

[2] D. S. Weile and E. Michielssen, "Genetic algorithm optimization applied to electromagnetics: A review," *IEEE Trans. Antennas Propagat.*, vol. 45, pp. 343–353, Mar. 1997.

[3] S. Charkravarty, R. Mittra, and N. R. Williams, "On the application of the microgenetic algorithm to the design of broad-band microwave absorbers comprising frequency-selective surfaces embedded in multilayered dielectric media," *IEEE Trans. Microwave Theory Tech.*, vol. 49, pp. 1050–1059, June 2001.

[4] D. S. Weile and E. Michielssen, "Design of doubly periodic filter and polarizer structures using a hybridized genetic algorithm," *Radio Sci.*, vol. 34, no. 1, pp. 51–63, Jan.-Feb. 1999.

[5] R. A. Hill and B. A. Munk, "The effect of perturbating a frequency selective surface and its relation to the design of a dual-band surface," *IEEE Trans. Antennas Propagat.*, vol. 44, pp. 368–374, Mar. 1996.

[6] T. K. Wu and S. W. Lee, "Multiband frequency selective surface with multiring patch elements," *IEEE Trans. Antennas Propagat.*, vol. 42, pp. 1484–1490, Nov. 1994.

[7] J. Huang, T. K. Wu, and S. H. Lee, "Tri-band frequency selective surface with circular ring elements," *IEEE Trans. Antennas Propagat.*, vol. 42, pp. 166–175, Feb. 1994.

[8] T. K. Wu, "Four-band frequency selective surface with double-square-loop patch elements," *IEEE Trans. Antennas Propagat.*, vol. 42, pp. 1659–1663, Dec. 1994.

[9] A. D. Chuprin, E. A. Parker, and J. C. Batchelor, "Convoluted double square: Single layer FSS with close band spacings," *Electron. Lett.*, vol. 36, pp. 1830–1831, Oct. 2000.

[10] J. Romeu and Y. Rahmat-Samii, "Fractal FSS: A novel dual-band frequency selective surface," *IEEE Trans. Antennas Propagat.*, vol. 48, pp. 1097–1105, July 2000.

[11] J. P. Gianvittorio, Y. Rahmat-Samii, and J. Romeu, "Fractal FSS: Various self-similar geometries used for dual-band and dual-polarized FSS," in *Proc. Int. IEEE AP-S Symp. Dig.*, July 2001, pp. 640–643.

[12] R. Mittra, C. H. Chan, and T. Cwik, "Techniques for analyzing frequency selective surfaces – A review," *IEEE Proc.*, vol. 76, no. 12, pp. 1593–1615, Dec. 1988.
[13] C. H. Chan and R. Mittra, "On the analysis of frequency-selective surfaces using subdomain functions," *IEEE Trans. Antennas Propagat.*, vol. 38, pp. 40–50, Jan. 1990.
[14] G. Manara, A. Monorchio, and R. Mittra, "Frequency selective surface design based on genetic algorithm," *Electron. Lett.*, vol. 36, no. 17, pp. 1400–1401, Aug. 1999.
[15] M. Ohira, H. Deguchi, M. Tsuji, and H. Shigesawa, "Optimized single-layer frequency selective surface and its experimental verification," in *European Microwave Conference Proceedings*, Sep. 2002, pp. 981–984.
[16] H. Choo and H. Ling, "Design of broadband and dual-band microstrip antenna on a high-dielectric substrate using a genetic algorithm," *Proc. Inst. Elect. Eng. Microw. Antennas Propag.*, vol. 150, no. 3, pp. 137–142, June 2003.
[17] A. S. Barlevy and Y. Rahmat-Samii, "On the electrical and numerical properties of high Q resonances in frequency selective surface," in *Progress in Electromagn. Res.*, J. A. Kong, Ed., 1999, vol. PIER 22, pp. 1–27.
[18] B. A. Munk, *Frequency Selective Surfaces: Theory and Design*. New York: Wiley, 2000.

Masataka Ohira (S'03) was born in Osaka, Japan, on July 21, 1978. He received the B.E. and M.E. degrees from Doshisha University, Kyoto, Japan, in 2001 and 2003, respectively.

Currently, he is a student of the Graduate School of Electric Engineering, Doshisha University. His current research activities are concerned with the analysis and design of the frequency selective surfaces and their application.

Mr. Ohira is a Member of the Institute of Electronics, Information and Communication Engineers (IEICE), Japan and the Institute of Electrical Engineers (IEE), Japan.

Hiroyuki Deguchi (M'92) was born in Osaka, Japan, on August 24, 1962. He received the B.E., M.E., and D.E. degrees from Doshisha University, Kyoto, Japan, in 1986, 1988, and 1999, respectively.

Between 1988 and 2000, he joined Mitsubishi Electric Corporation, where he had been engaged in research and development of very large reflector antennas, deployable antennas, horn antennas, and radome antennas. Since 2000, he has been with Doshisha University, where he is currently an Associate Professor. His current research activities are concerned with microwave and millimeter-wave aperture antennas and antenna measurements.

Dr. Deguchi is a Member of the Institute of Electronics, Information and Communication Engineers (IEICE), Japan and the Institute of Electrical Engineers (IEE), Japan. He received IEICE Young Engineer Award in 1992.

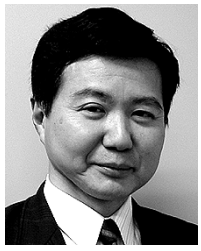

Mikio Tsuji (S'77–M'82) was born in Kyoto, Japan, on September 10, 1953. He received the B.E., M.E., and D.E. degrees from Doshisha University, Kyoto, Japan, in 1976, 1978, and 1985, respectively.

Since 1981, he has been with Doshisha University, where he is now a Professor. His present research activities are concerned with microwave and millimeter-wave guiding structures and devices and scattering problems of electromagnetic waves.

Dr. Tsuji is a Member of the Institute of Electronics, Information and Communication Engineers (IEICE) of Japan and the Institute of Electrical Engineers (IEE) of Japan.

Hiroshi Shigesawa (S'62–M'63–SM'85–FM'94) was born in Hyogo, Japan, on January 5, 1939. He received the B.E., M.E., and D.E. degrees from Doshisha University, Kyoto, Japan, in 1961, 1963, and 1969, respectively.

Since 1963, he has been with Doshisha University. From 1979 to 1980, he was a Visiting Scholar at the Microwave Research Institute, Polytechnic Institute of New York, New York. Currently, he is a Professor in the Faculty of Engineering, Doshisha University. His present research activities involve microwave and millimeter-wave guiding structures and devices and scattering problems of electromagnetic waves.

Dr. Shigesawa is a Member of the Institute of Electronics, Information and Communication Engineers (IEICE) of Japan, the Institute of Electrical Engineers (IEE) of Japan, and Optical Society of America (OSA).